IOSR Journal of Mechanical and Civil Engineering (IOSR-JMCE)
e-ISSN: 2278-1684,p-ISSN: 2320-334X, Volume 16, Issue 5 Ser. III (Sep. - Oct. 2019), PP 52-65
www.iosrjournals.org

Ultimate Behaviour of Prestressed Box Girder Cable Stayed Bridges

Ayman M. Ismail[1], Ahmed Mohey Ibrahim[2], khaled Elbadry[3]
[1]*Dean of Pyramids Higher Institute of Engineering and Technology, Professor of Structural Engineering, HBRC, Egypt,*
[2]*Doctor of Structural Engineering, HBRC, Egypt,*
[3]*Doctor of Structural Engineering, HBRC, Egypt,*
Corresponding Author: Ayman M. Ismail

Abstract: *The study described here investigates the nonlinear static and ultimate behaviour of Box girder Cable stayed bridge up to failure. The nonlinear stress-strain behaviour, together with distortion and warping are considered for more accurate analysis of prestressed single box-girder cable stayed bridges. Concrete cracking moment and ultimate strength are determined in order to confirm the structure capacity against failure. The interaction between concrete and reinforcing steel due to the tension stiffening related with concrete cracking is also considered.*

Keywords: *Ultimate, Prestressed, Box Girder, Cable Stayed Bridges,*

Date of Submission: 7-10-2019 Date of Acceptance: 23-10-2019

I. Introduction

During the last three decades, there has been increasing interest in the field of cable stayed bridge systems all over the world. Researchers have developed different techniques of analysis and have considered many aspects of nonlinearity.

In a simplified approach, the cable-stayed bridge is assumed a linear elastic system, which may be analyzed using the standard stiffness or flexibility methods. Tang (1971) has applied the transfer matrix method to nonlinear analysis of cable-stayed bridges in which a modified modulus of elasticity was used. Lazar (1972) studied the linear and nonlinear analyses using the stiffness matrix method. The nonlinear effects due to large deformations, the interaction of axial forces and bending moments, and due to the catenary's effect of cables were considered. Fleming and Egeseli (1979) presented a combined incremental and iterative approach for two and three-dimensional nonlinear analyses of cable stayed bridges. Podolny and Scalzi (1986) presented influence lines for different cable arrangements. Seif and Dilger (1990) investigated both geometric and material nonlinearities and concluded that the material nonlinearity was dominant in the nonlinear static behavior of long span cable stayed bridges. The failure criteria adopted by Seif and Dilger is the formation of a plastic hinge. Troitsky (1999), Wilson and Gravelle (1991), and Xanthakos (1993) reported that one could ignore cables nonlinearity by linearization of cables' stiffness, using an equivalent modulus of elasticity.

II. Nonlinear Analysis

Cable-stayed bridges exhibit geometric nonlinearity due to: (1) The nonlinear axial force elongation behavior for the inclined cable stays under different tension load levels due to the sag initiated by their own weight (sag effect), (2) the combined axial load and bending moment interaction for both girder and tower elements, and (3) large displacement associated with the geometrical changes of the structure. Under service load, it is sufficient to account for geometric nonlinearity, but near failure, load material nonlinearity must also be considered.

II.1 Geometric Nonlinearities

The most known cause of geometric nonlinearity of the system is the sagging of the cables. The axial stiffness of a stay cable depends on two factors; (1) the sag of the cable and (2) its axial deformation. The sag has a softening effect on the cable stiffness, which results in a nonlinear axial force-displacement relationship. The cable has a low stiffness for relatively large values of the sag, however as the sag decreases the cable stiffness increases and the behavior of the cable approaches that of a truss bar in tension.
Referring to figure (1), the secant modulus, Esec is given by (John 1988):

$$\frac{1}{E_{sec}} = \frac{1}{E} + \frac{(\gamma\cos\phi)^2\ell^2}{24}\left(\frac{\sigma_1+\sigma_2}{\sigma_1^2.\sigma_2^2}\right) \quad (1)$$

Where **E** is the modulus of elasticity, γ is the weight density, **I** is the chord length, ϕ is the cable angle of inclination, σ□ and σ2 are cable stresses in points 1 and 2 along the cable respectively.
To determine the secant modulus the cable stresses σ□ and σ2 must be known. In most cases σ2 is not known and has to be estimated resulting in an iterative procedure.
Substituting σ2 = σ□ into equation (1), the tangent modulus Etan is given by:

$$E_{tan} = \frac{E}{1+\left[\frac{E(\gamma\cos\phi)^2\ell^2}{12.\sigma_1^3}\right]} \quad (2)$$

In this study, the tangent modulus is used for an initial estimate of the cable stiffness.

The second source of geometric nonlinearity is the combined axial force and bending moment effect. The presence of axial force affects the stiffness of the non-prismatic trapezoidal box beam element used in modeling the deck and the tower. The last source of geometric nonlinearity is due to the large deflection of the structure. Like all nonlinear structural analysis problems, the nonlinear analysis of long span cable stayed bridges finally reduces to forming nonlinear incremental equilibrium equations of the system and to solving these equations.

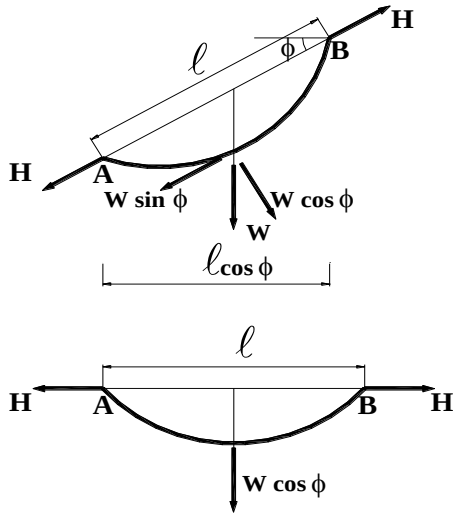

Fig. 1.a Inclined Stay Cable and Equivalent Horizontal Stay Cable With Equal Deformational Characteristics

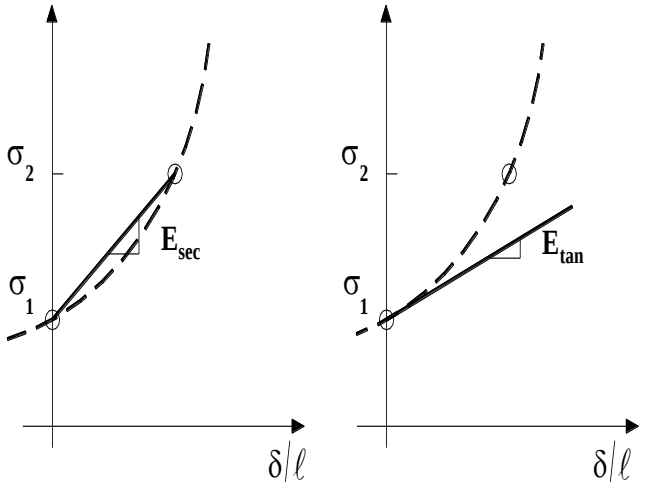

Fig. 1.b Linearized Force-Displacement Relationships; Secant and Tangent Stiffness of a Stay Cable

II.2 Material Nonlinearities

For elastic analysis under working loads, linear idealization is universally accepted. However, for the analysis of structures under overload up to collapse, nonlinear behavior for both concrete and steel must be considered.

In this study, the mathematical model adopted for the stress strain curve of concrete is the one suggested by Kang (1977,1989) as shown in figure (2). A simple load reversal model in the stress strain curve accounts for loading and unloading. For this model it is assumed that the slope in the load reversal path is the same as the initial tangent modulus Ei , and that tensile failure or cracking of concrete occurs when tensile stress exceeds its maximum tensile strength f\t . Once concrete has cracked, it cannot take any tensile stress again, but it can take compressive stresses upon closing of the crack. Thus the crack is assumed to close in compression and reopen in tension without any resistance. Also concrete is defined as yielded when its compressive mechanical strain exceeds εo which is the strain corresponding to the maximum compressive stress f"c , whereas compressive failure or crushing of concrete occurs when the compressive mechanical strain exceeds the maximum compressive strain εu.
The parameters necessary to define this concrete stress-strain curve are the initial tangent modulus Ei, the maximum compressive strength f"c , the maximum tensile strength f\t and the ultimate strain εu. With lack of

experimental data, those parameters may be obtained using different codes of practice. Recommendations of the ACI Committee 209 (1997) are frequently used for bridge design.
The complete stress-strain relationship of concrete can be summarized by the following equations:
Region (1):

$$\sigma = E_i \ . \ \varepsilon^m \qquad (3)$$

Region (2):

$$\sigma = f_c^{"} \ \frac{\varepsilon^m}{\varepsilon_o} \left(2 \ - \ \frac{\varepsilon^m}{\varepsilon_o} \right) \qquad (4)$$

Region (3):

$$\sigma = f_c^{"} \ - \ 0.15 \ f_c^{"} \ \frac{\varepsilon^m \ - \ \varepsilon_o}{\varepsilon_u \ - \ \varepsilon_o} \qquad (5)$$

Regions (6) and (7):

$$\sigma = E_i \ \left(\varepsilon^m \ - \ \varepsilon_r \right) \qquad (6)$$

Where ε_r is the residual strain due to unloading.

For the reinforcing steel, a bilinear model, which is symmetrical about the origin as shown in figure (3), is used in this study. The load reversal path is assumed to stay within the envelope indicated by the dotted lines and failure is assumed to occur when the mechanical strain εm exceeds the ultimate strain εu . Four different material states can be identified in the stress-strain curve and the corresponding equations can be written as follows:
Case (1): In primary tension or compression

$$\sigma = E_1 \ . \ \varepsilon^m \qquad (7)$$

Case (2): Yielded

$$\sigma = E_2 \ . \ \varepsilon^m \ \pm \left(\ \sigma_y \ - \ E_2 \ . \ \varepsilon_y \right) \qquad (8)$$

Case (3): In the load reversal path

$$\sigma = E_1 (\varepsilon^m - \varepsilon_r) \qquad (9)$$

Case (4): Failed

Where E_1 is the initial modulus up to yielding, E_2 is the second modulus after yielding, σ_y is the yield stress, ε_y is the yield strain and εr is the residual strain due to load reversal.

A multi linear stress strain curve as shown in figure (4) is adopted for the prestressing steel, where the slope of each of the unloading and reloading path is assumed the same as the initial modulus. Since the prestressing steel is never subjected to compressive stresses the compressive stress strain curve is not considered. The state of stress is given by the following equations:

$$\sigma_j = \sigma_{(j-1)} + E_j \left(\varepsilon_j^m \ - \ \varepsilon_{(j-1)} \right) \quad , j= 1,2,... \qquad (10)$$

$$\sigma = E_1 \left(\varepsilon^m \ - \ \varepsilon_r \right) \quad \text{on load reversal path} \qquad (11)$$

As for cables, the algorithm used in this study to determine the nonlinear material state is best explained by an example as follows:
(1) Assume that the cable steel has a tri-linear stress strain curve as shown in figure (5.a). Further, assume that the cable has a chord length I and a weight density γ , and let the initial stress in the cable be σ_0 .
(2) Generate the stress (σ) versus the apparent strain ($\hat{\varepsilon}$) curve shown in figure (5.b), where the strain($\hat{\varepsilon}_j$) corresponding to the stress σ j is given by (Seif and Dilger,1990):

$$\hat{\varepsilon}_j = \frac{\delta_j}{\ell} = \frac{(\sigma_j - \sigma_{j-1})}{E_j} + \frac{\gamma^2 \ell^2}{24} \left[\frac{1}{\sigma_{j-1}^2} - \frac{1}{\sigma_j^2} \right] \qquad (12)$$

(3) Assume that an element end axial displacement δ is imposed, and compare δ with the ($\delta_1, \delta_2, \delta_3$) array. For example if δ is such that $\delta_1 < \delta < \delta_2$, then the new total stress in the cable is given by:

$$\sigma = \sigma_1 + \hat{\sigma} \quad \text{, where} \qquad (13)$$

$$\frac{\delta - \delta_1}{\ell} = \frac{\hat{\sigma} - \sigma_1}{E_2} + \frac{\gamma^2 \ell^2}{24}\left[\frac{1}{\sigma_1^2} - \frac{1}{\hat{\sigma}^2}\right] \qquad (14)$$

Equation (14) is solved for $\hat{\sigma}$ using the Newton-Raphson method.

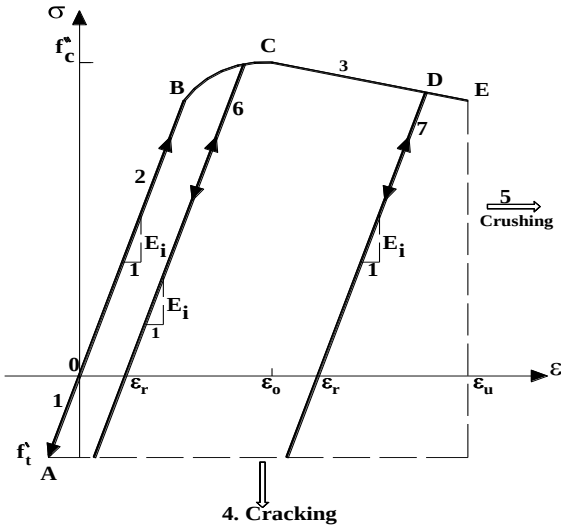

Fig. 2 Stress Strain Curve of Concrete

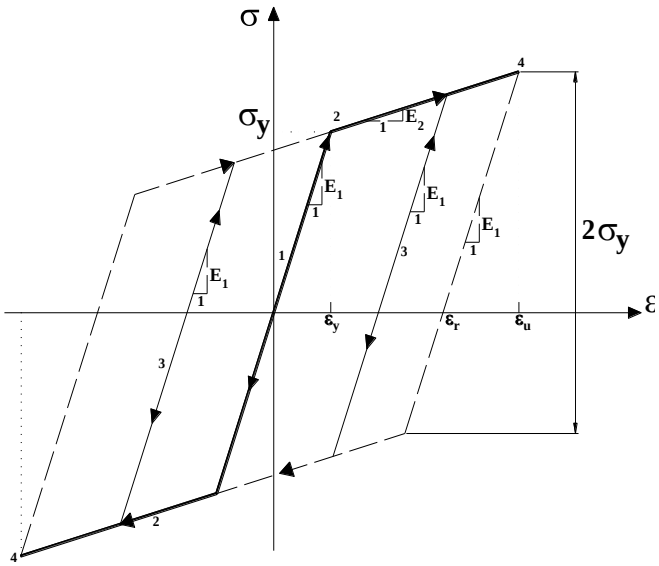

Fig. 3 Uni-axial Stress Strain Curve of Reinforcing Steel

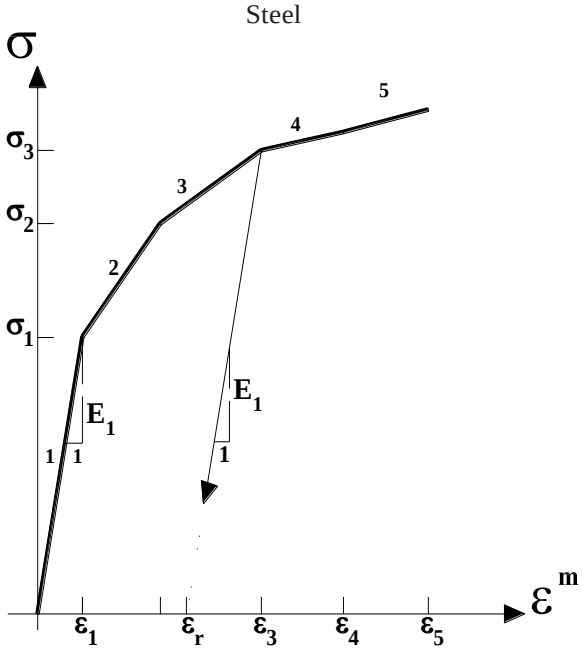

Fig. 4 Uni-axial Multi Linear Stress Strain Curve of Prestressing Steel

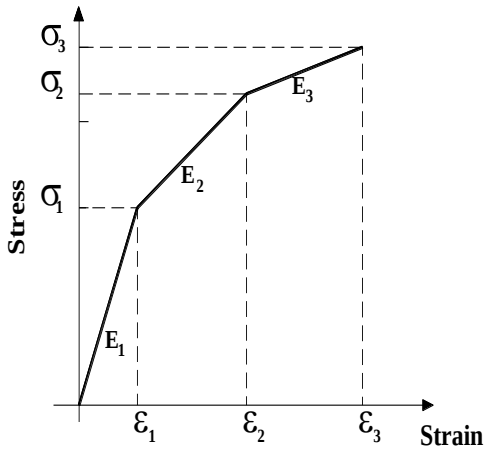

Fig. 5.a Tri-Linear Stress Strain Curve of the Cable Steel

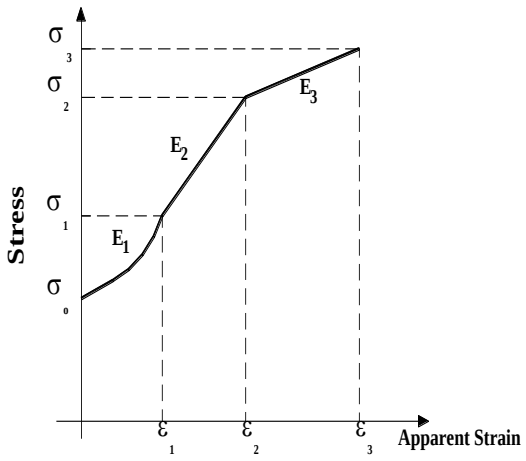

Fig. 5.b Stress Vs Apparent Strain Plot of the Stay Cable

1)

III. Bridge Modeling

The bridge deck and towers are modeled using a non-prismatic thin-walled trapezoidal box beam element. This element has eight displacement modes (DOF) at each node to account for the transverse distortion and the longitudinal warping. The formulation is based on the finite element method combined with the thin-walled beam theory. The reinforcing steel and the prestressing steel tendons are also considered. Ismail (2002) gives a detailed discussion of the derivation of the element tangent stiffness matrix, the internal forces and the initial strain load vector. Stay cables are modeled using a combined element of an inextensible cable, which models the sag effect, and an elastic truss element (Seif and Dilger, 1990).

IV. Case Studies

Three different types of cable-stayed bridges are analyzed using the developed computer program (Ismail, 2002). Cable stays are arranged in a symmetric radiating pattern, fan pattern or harp pattern. All three bridges are assumed to have the same span length and same geometric and materials properties. The dead load is first applied to the bridge, then a uniformly distributed load is applied to the deck in increments until maximum capacity of the bridge is reached. The ultimate strength of the bridge is achieved when an equivalent failure mechanism occurs. The deflected shapes of the bridge under the dead load effect, at the formation of the first plastic hinge (when the maximum capacity of deck cross section is reached) and under the ultimate load effect are plotted. Bending moments due to dead load, uniformly distributed service load (according to AASHTO specifications) and at ultimate load are obtained.

IV.1 Bridge Geometry and Material Properties

Geometry of the bridge and the properties of the used materials are adapted from a technical publication by Seif and Dilger (1990). The bridges have a central span of 200m and two side spans of 90m each, while the total height of the towers is 82m. The deck consists of 19.2m wide and 2.0m deep reinforced prestressed concrete box girder segments. The closure segment in the middle of the central span is 20m long while other segments are 15m long. Each segment is supported by a cable, which in turn is anchored to the tower. The towers are H- shaped and each leg of the H consists of a reinforced concrete single box girder section. The deck is supported at the tower by means of a roller bearing and its movement in the longitudinal direction is only constrained by the cable stays. Figure (6) shows the three bridge models while figure (7) shows the cross sections of the bridge deck and tower.

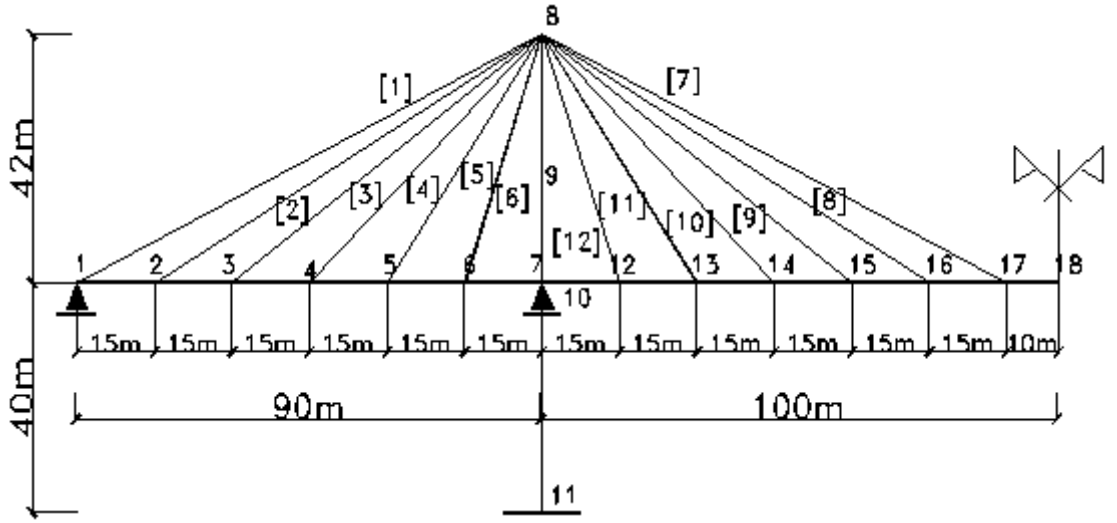

Fig. 6.a Radiating Cable-Stayed Bridge Model

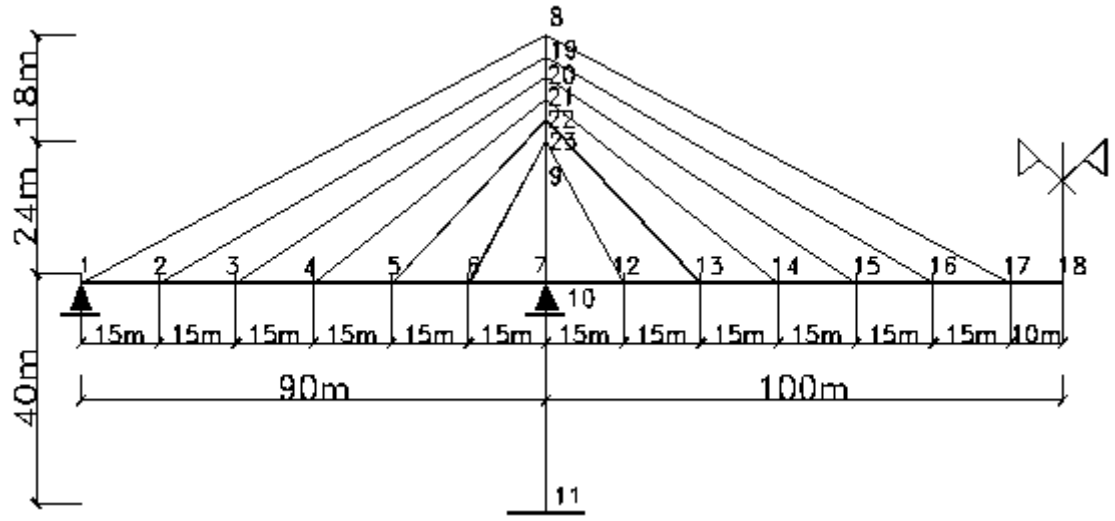

Fig. 6.b Fan Cable-Stayed Bridge Model

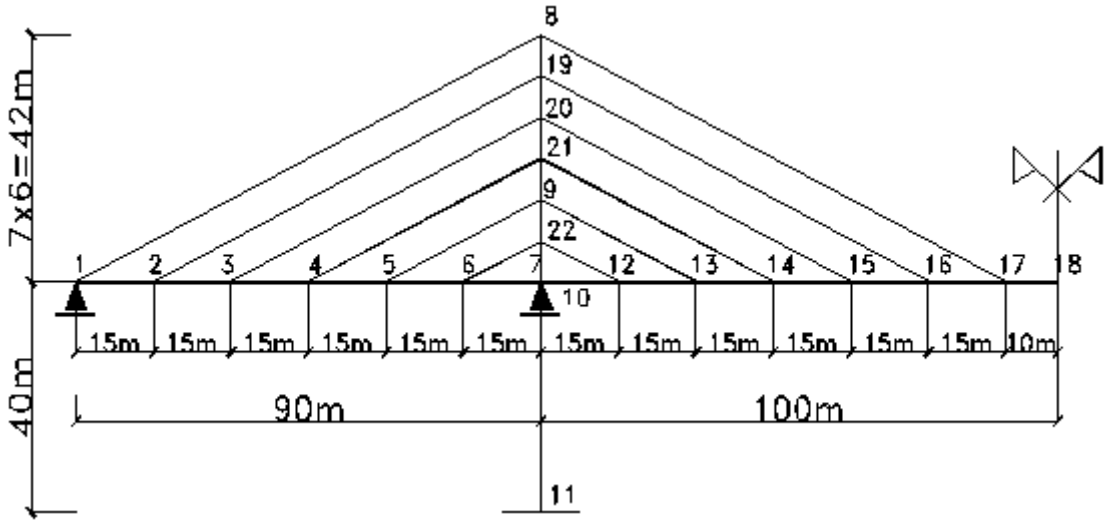

Fig. 6.c Harp Cable-Stayed Bridge Model

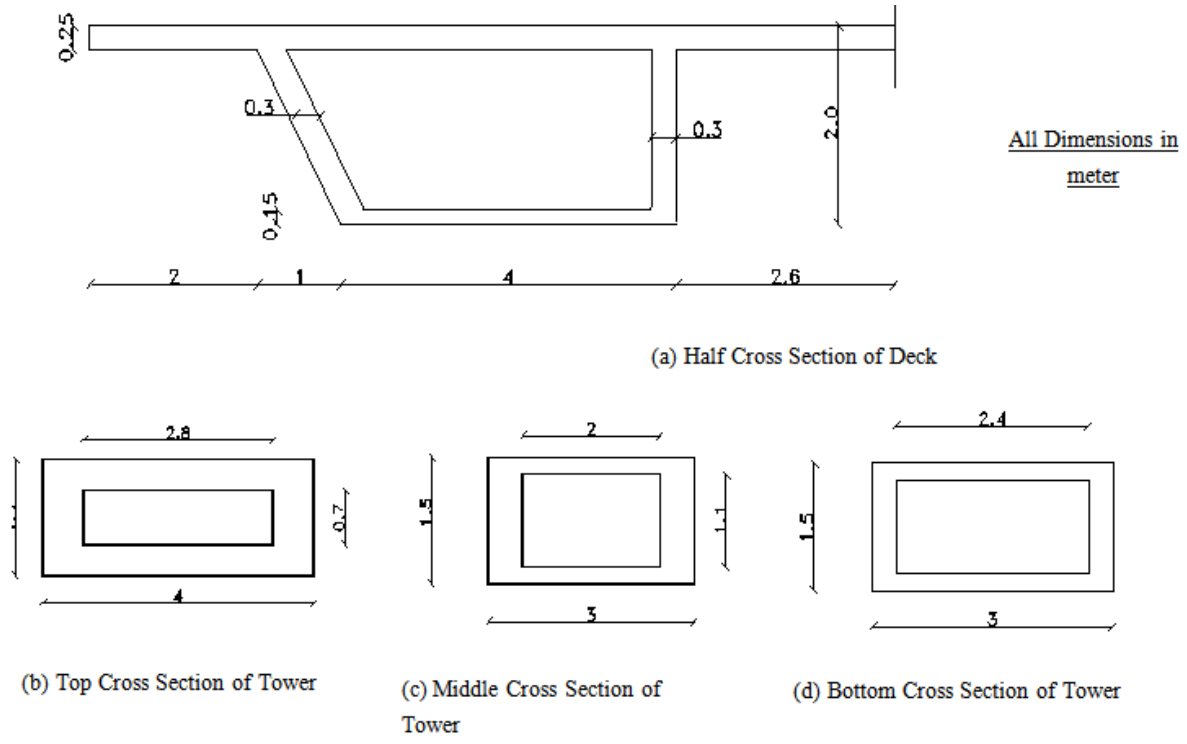

Fig. 7 Cross Sections of Bridge Deck and Tower

Deck and tower concrete has a maximum cylinder compressive strength of fc'= 40 MPa, a modulus of elasticity Ec= 30000 MPa, and an ultimate strain εu = 0.0035. The steel reinforcement has a yield strength fy = 400 MPa, moduli of elasticity Es1 = 200000 MPa and Es2 = 930 MPa and an ultimate strain εu =0.0300 . Both the cable steel and, modulus of elasticity, the prestressing steel have a multi-linear stress strain curve, and the coordinates of the ends of each linear segment are given in tables (1) and (2).

Table (1) Stress Strain Curve Data of the Stay Cables Steel

Point No.	Stress (MPa)	Strain
1	1240	.0072
2	1447	.0088
3	1653	.0120
4	1722	.0160
5	1860	.0500

Table (2) Stress Strain Curve Data of the Deck Prestressing Steel

Point No.	Stress(MPa)	Strain
1	1354	.0072
2	1516	.0090
3	1653	.0115
4	1688	.0135
5	1860	.0580

Table (3) gives the cables areas and initial forces. It is to be noted that each cable initial force is applied such that its vertical component is equal to the deck dead load supported by the cable at the cable node. The reinforcement of the deck cross section is As1=150 cm2, As2=50 cm2 and As3=150 cm2 arranged in the top flange, each web and each bottom flange respectively. The deck prestressing tendons are post tensioned and have a linear profile, which coincides with the centroid of the concrete section. The cross section of each tendon is 80 cm2 and the prestressing force is equal to 820 kN. Tendons are extended between nodes 1&18, 14&18 and 16&18. The reinforcement of the tower box sections is As1= As2=100 cm2 and As3=160 cm2 arranged in the top, middle and bottom cross sections respectively.

Table (3) Cross Sectional Areas and Initial Forces in the Stay Cables

Cable No.	Cross Sectional Area, x103 (mm2)	Initial Tension (Prestress) (kN)		
		Radiating	Fan	Harp
1	10	4340	4340	4340
2	10	3480	3722	4020
3	5	2522	2870	3420
4	5	2219	2640	3580
5	5	1840	2194	3540
6	5	1590	1755	3540
7	10	4340	4340	4340

8	10	2848	3046	3290
9	5	2622	3029	3610
10	5	2188	2603	3530
11	5	1840	2194	3540
12	5	1590	1755	3540

IV.2 Ultimate Load Analysis

Figure (8) shows the deflected shape of the radiating type bridge under the effect of different load levels. The first plastic hinge is formed at the mid span of the bridge when 1.78 times the dead load is applied. A kink of a hinge in the deck profile at each of nodes 7 and 7/ is clear, indicating occurrence of an equivalent failure mechanism, when the applied load reaches 3.75 times the dead load. Figure (9) shows the bridge deck bending moments under the effect of different load levels. It is to be noted that under the dead load effect the positive moment at the mid span and the negative moment at the tower support are approximately equal and larger than the bending moments at the rest of the deck nodes. As the load increases the negative moment at node 7 increases much more rapidly than the positive moment at node 18.

Figure (10) shows the deflected shape of the fan type bridge under the effect of different load levels. The first plastic hinge is also formed at the mid span of the bridge when 1.76 times the dead load is applied. An equivalent failure mechanism occurs when the bridge deck is subjected to a uniform load equals 3.5 times the dead load. Figure (11) shows the bridge deck bending moments under the effect of different load levels.

Figure (12) shows the deflected shape of the harp type bridge under the effect of different load levels. Two plastic hinges are formed at the quarter points of the middle span of the bridge deck when 2.56 times the dead load is applied. The bridge fails when 2.83 times the dead load of the bridge deck is applied. Figure (13) shows the bridge deck bending moments under the effect of different load levels.

Figure (14) shows the mid span deflection for different dead load multipliers up to failure for the three bridges. It can be observed that the radiating type bridge can resist loads 33% higher than the harp type. It can also be seen that the behavior of the harp type differs from that of the radiating and the fan types when the plastic hinges are formed due to the change of the structural system. Figure (15) shows the deflected shape of the bridge deck under the effect of the service load for the three bridges. The mid span deflection of the radiating type is 25% less than that of the harp type. The remarkably less deflected shape of the radiating type than that of the harp type indicates that the radiating type resists higher loads than the harp type. This occurs because the cables inclinations are higher for the radiating type. It is clear that an increase in the cable inclination increases its ability to resist the acting vertical loads. Figure (16)shows the ultimate bending moment diagrams for the three bridges. Comparison of results shows that the maximum bending moment at the central span is 50% higher for the radiating type than the harp type, which indicates the higher resistance of the radiating type. Figure (17) shows the cables forces under the effect of the ultimate loads for the three bridges. It can be observed that the radiating type resists more loads through the cables than the harp type, and that the largest gain in the cables forces occurred in the end cables (1, 2, 7 and 8). It is to be noted that under the effect of the ultimate loads the stresses in the stay cables of the three bridges did not exceed the yield strength.

It is to be noted that Seif and Dilger (1990) investigated the ultimate capacity of the same three bridge types. A spaces frame element has been used to model the bridge deck and tower, and the formation of a plastic hinge in the bridge deck defined the ultimate strength of the bridge. Comparison with Seif and Dilger results shows an increase of 5% in the bridge capacity. In the current study the accuracy of the bridge deck and tower modeling and the ability of increasing the applied load after the formation of the plastic hinges enhances the analysis, and higher ultimate capacity of the bridge is obtained.

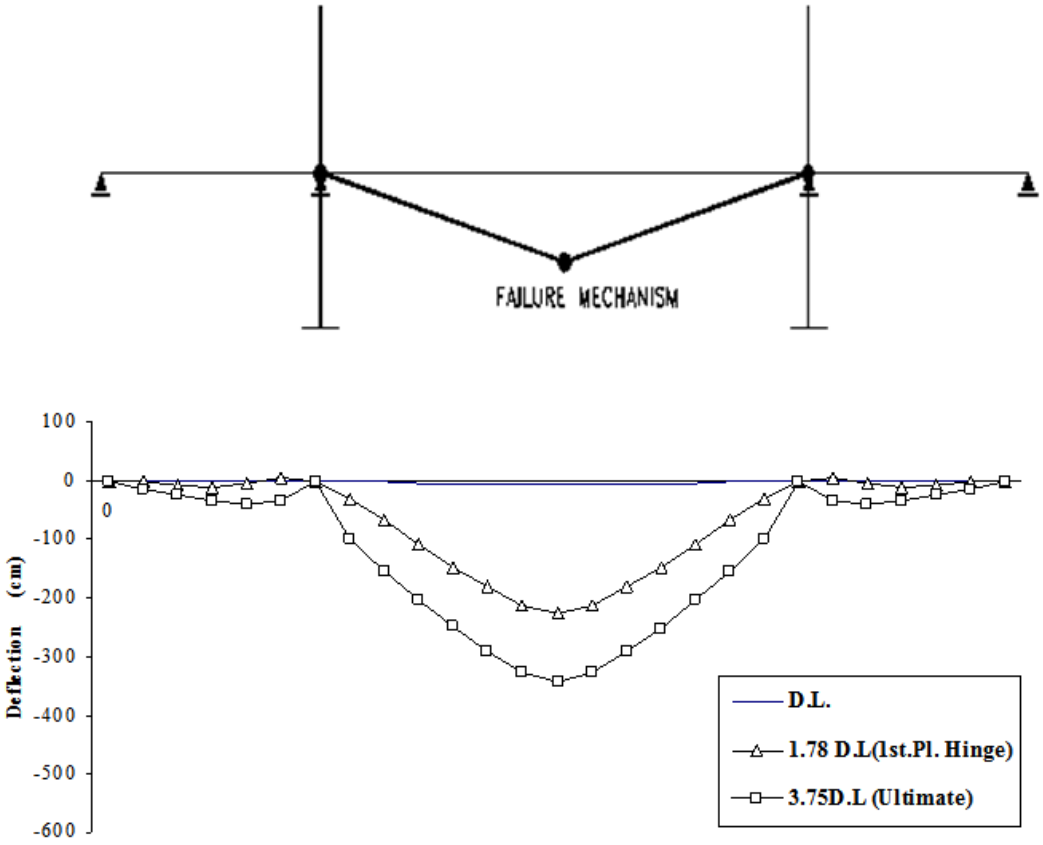

Fig. 8 Deflected Shape of Bridge under the Effect of Different Load levels (Radiating Type)

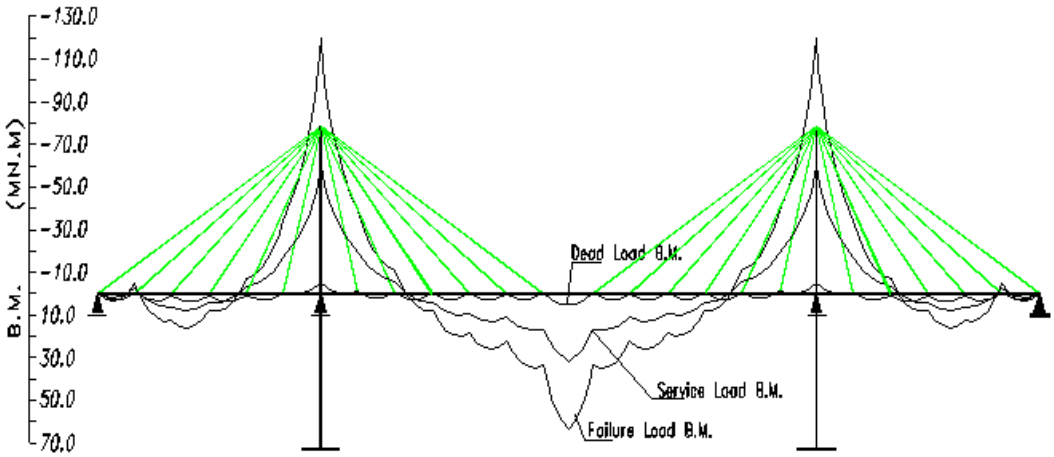

Fig. 9 Bending Moment Diagrams (Radiating Type)

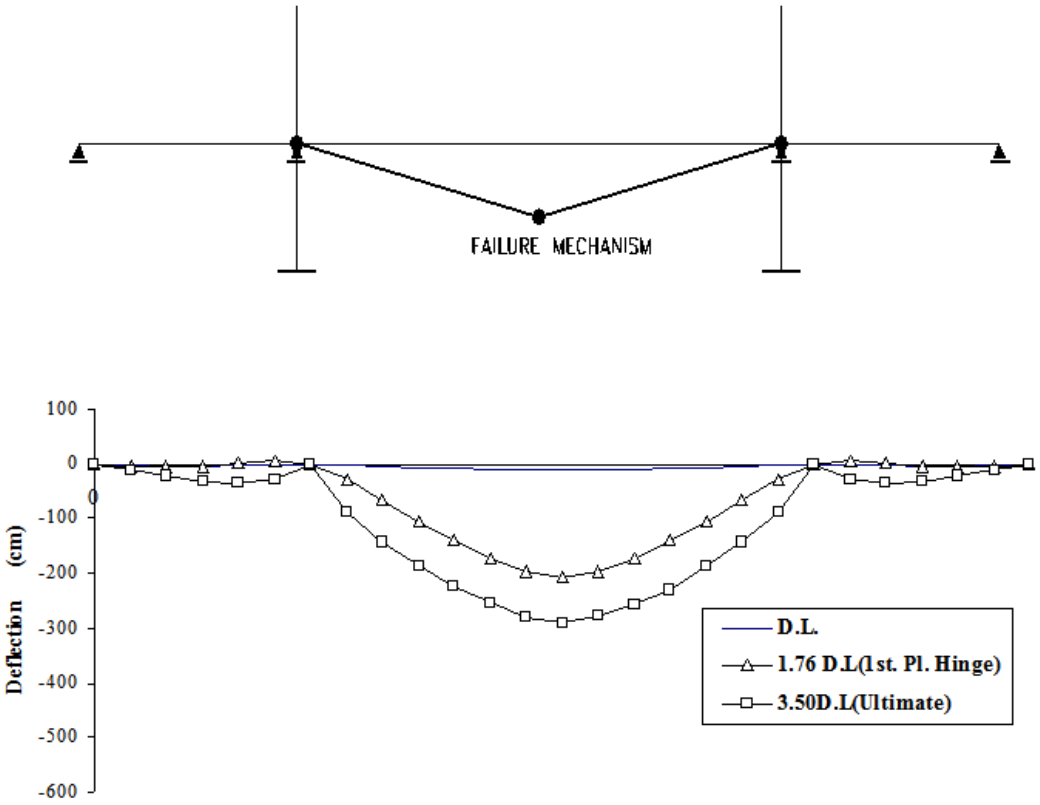

Fig. 10 Deflected Shape of Bridge Under the Effect of Different Load levels (Fan Type)

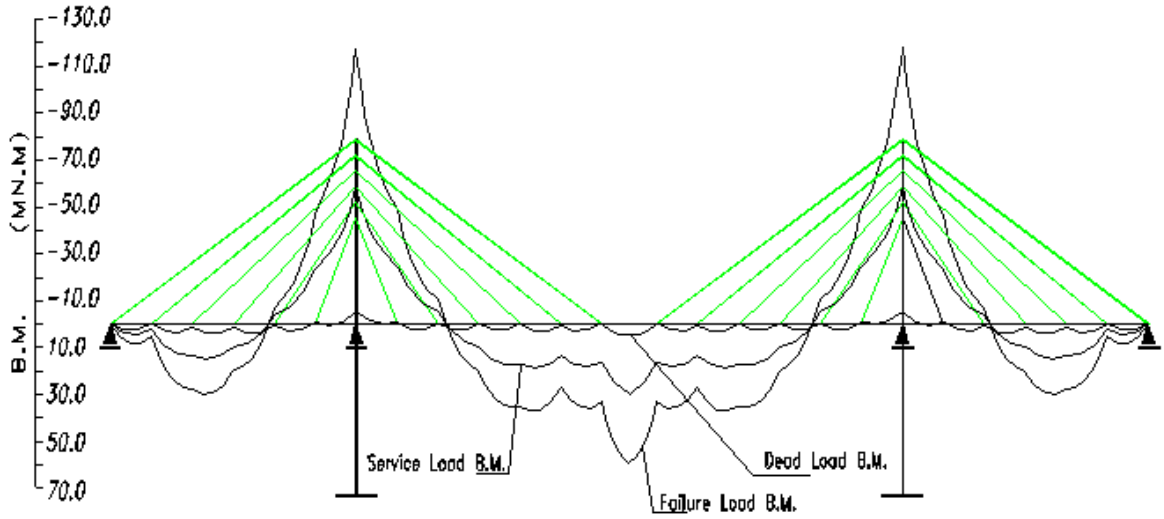

Fig. 11 Bending Moment Diagrams (Fan Type)

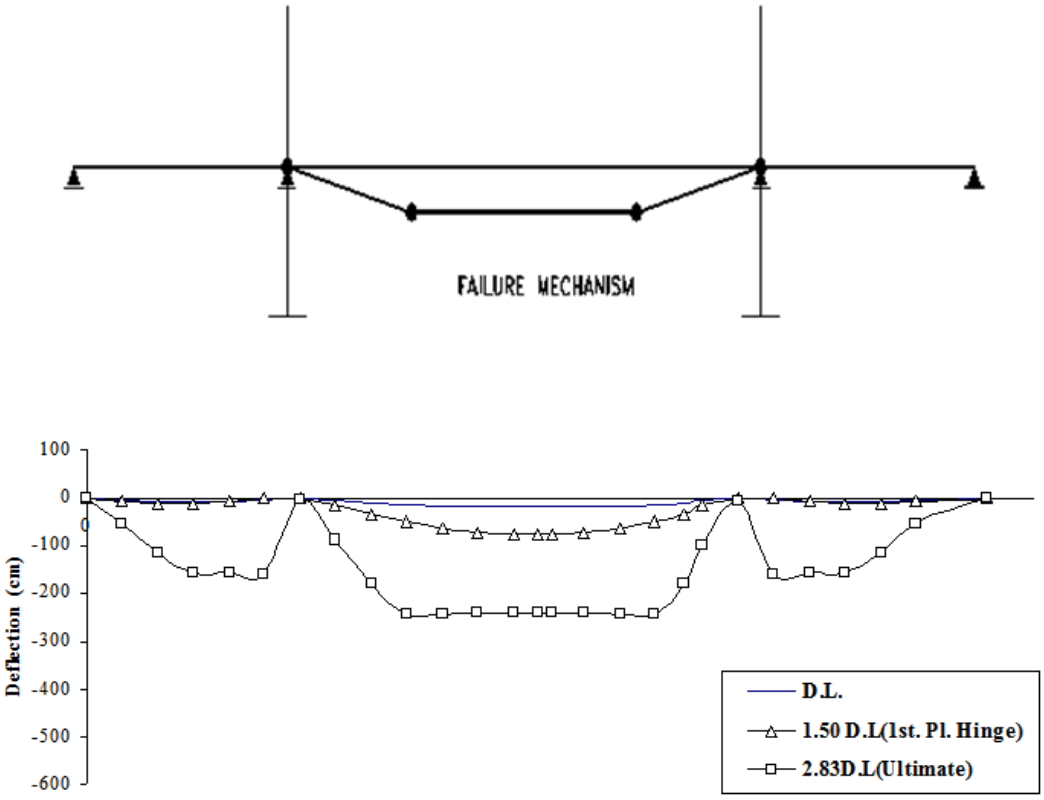

Fig. 12 Deflected Shape of Bridge Under the Effect of Different Load levels (Harp Type)

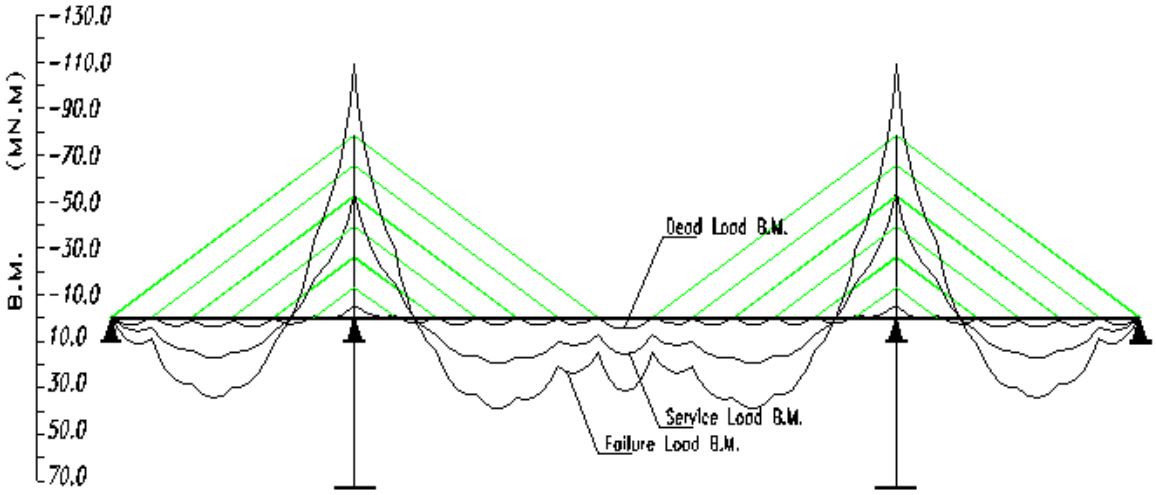

Fig. 13 Bending Moment Diagrams (Harp Type)

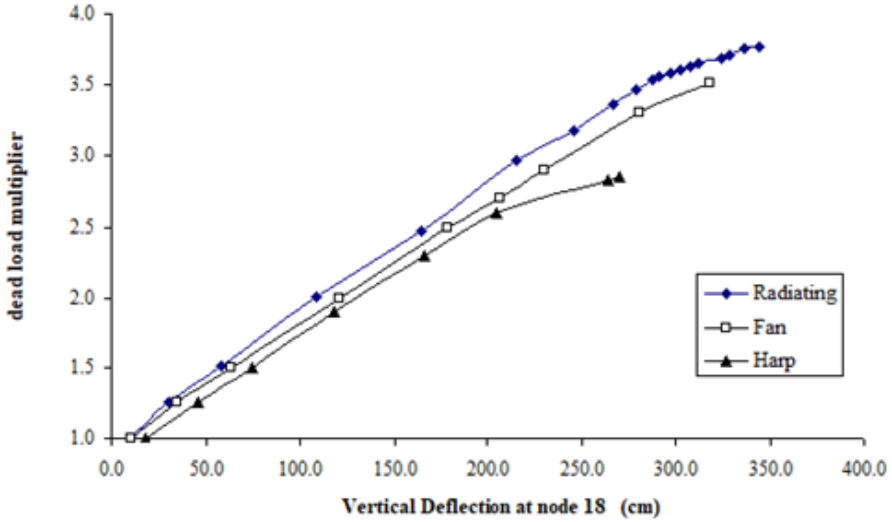

Fig. 14 Mid Span Deflection for Different Dead Load Multipliers for the Three Bridges

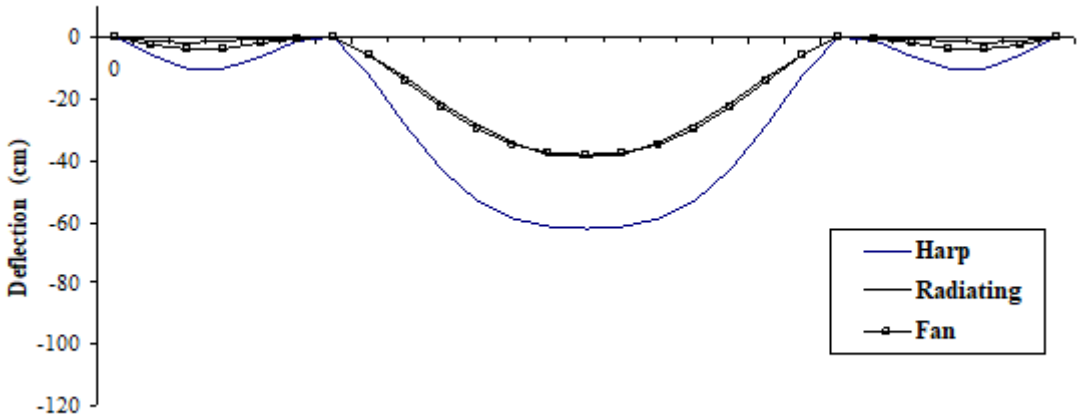

Fig. 15 Deflected Shape of the Bridge Deck Under the Effect of Service Load for the Three Bridges

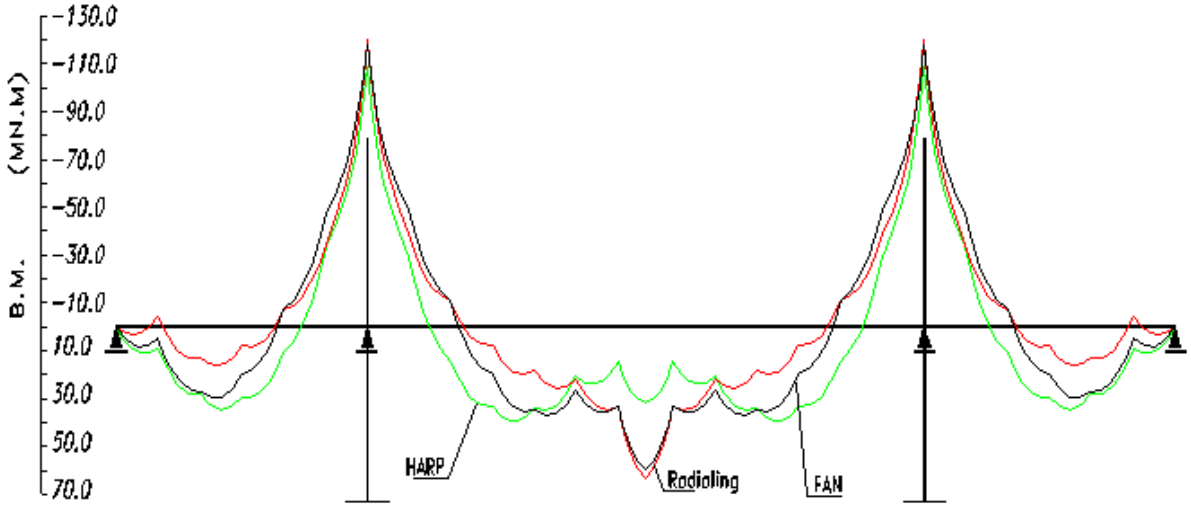

Fig. 16 Ultimate Bending Moment Diagrams for the Three Bridges

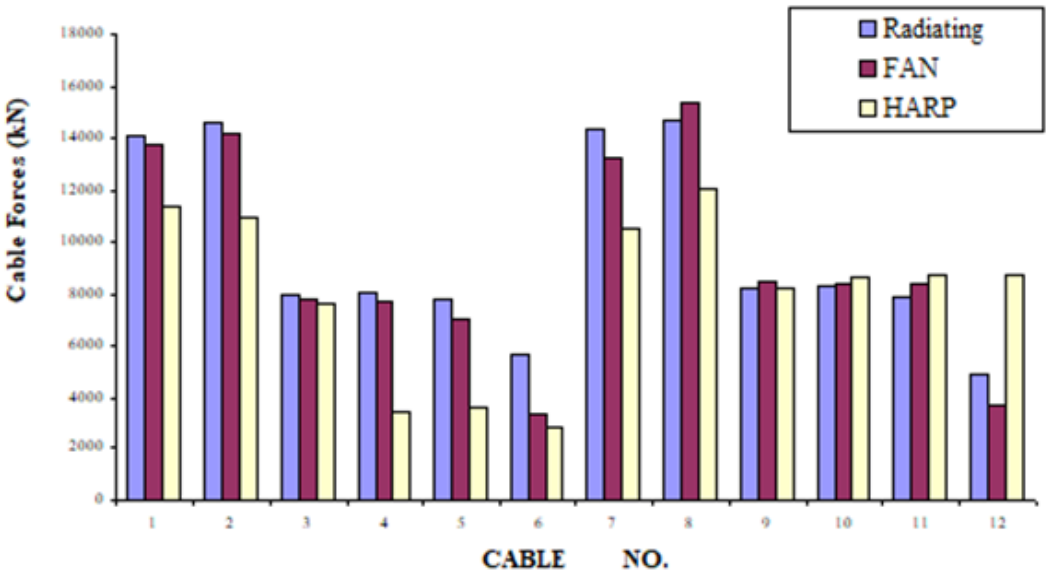

Fig. 17 Cables Forces Under the Effect of Ultimate Loads for the Three Bridges

V. Summary And Conclusions

A developed nonlinear finite element computer program was used to investigate the static nonlinear behaviour of box girder cable stayed bridges up to failure. Both geometric and material nonlinearities are considered. A non-prismatic thin-walled trapezoidal box beam element, which takes into account the transverse distortion and the longitudinal warping, was used to model the bridge deck and towers. Three case studies; radiating type, fan type and harp type cable stayed bridges were investigated under the effect of an incremental uniformly distributed load until the ultimate strength of the bridge is achieved when an equivalent failure mechanism occurs.

Comparison of results shows that for cable stayed bridge systems with the same bridge geometry and cross sectional and material properties of deck, towers and cables, the radiating type of cable arrangement is superior to other types of stay cable layouts. For the particular data used in this study, the radiating type system resists a failure load 33% higher than that of the harp type because the cables angles of inclination are higher. The increase in the slope of the cables increases their ability to resist the applied loads. On the other hand the radiating type requires more stay cable lengths than the fan or harp types. Moreover, the design and construction of the tower head for the radiating type is more complicated and costly.

At the same load level, the internal forces in the deck are higher for the harp type than those of the radiating type. On the other hand, the radiating type resists more loads through the cables. Under the effect of service loads the mid span deflection of the radiating type is 25% less than that of the harp type.

Comparison with published results showed good correlation. The accuracy of the bridge modeling and the ultimate behavior analysis emphasize the enhancement achieved in this current study.

Acknowledgements

We would like to express our deepest appreciation to Prof. M. Noor Fayed , Prof. Abdel-Salam Mokhtar (Professors of Structural Engineering, Civil Engineering Department, Ain Shams University) and Prof. M. Nabeel Abdel-Salam (Prof. of structural Engineering Housing & Building Research Center) For Their valuable help and support.

References

[1] Fleming, J. F., and Egeseli, E. A., "Dynamic Behaviour of a Cable-Stayed Bridge", Computers & Structures Vol. 10 No.4, 1979, pp. 621-635.
[2] Ismail, A.M., "Nonlinear Analysis of Bridge Girders Under Static and Dynamic Loads", Ph.D. Dissertation, Ain Shams University, Cairo, Egypt, 2002.
[3] John W. L., "Tension Structures, Behaviour & Analysis", Coolin Professional and Technical Books, UK, 1988.
[4] Kang, Y. J., "Nonlinear Geometric, Material and Time-Dependent Analysis of Reinforced and Prestressed Concrete Frames", Structural and Material Research Report No. UC-SESM 77-1, University of California, Berkeley, Jan.1977.
[5] Kang, Y. J., "SPCFRAME - Computer Program for Nonlinear Segmental Analysis of Planar Prestressed Concrete Frames", Report No. UC-SESM 89/07, University of California, Berkeley, Feb. 1989.
[6] Lazar, B.E., "Stiffness Analysis of Cable-Stayed Girder Bridges", Journal of the Structural Division, ASCE, Vol. 98, No. ST7, Sept. 1972, pp.2008-2020.
[7] Podolny, W., and Scalzi J. B., "Construction and Design of Cable-Stayed Bridges", Wiley, New York, 2nd. Ed. 1986.

[8] Seif., S.P., and Dilger, W.H., "Nonlinear Analysis and Collapse Load of PC Cable Stayed Bridges", Journal of Structural Engineering, ASCE, Vol. 116, No. 3, Mar. 1990, pp.829-849.
[9] Tang M. C., "Design of Cable-Stayed Bridges", Journal of Structural Engineering, ASCE, Vol. 97, No. ST5, May 1971, pp. 980-997.
[10] Troitsky, M. S., "Cable-Stayed Bridges, Theory and Design", Crosby Lockwood Staples, London, 1999.
[11] Wilson, J., and Gravelle, W., "Ambient Vibration Measurement and a Cable-Stayed Bridge", Earthquake Engineering & Structural Dynamics, Vol. 20, No. 8, 1991.
[12] Xanthakos, P. P., "Theory and Design of Bridges," Wiley, New York, 1993.

Ayman M. Ismail. "Ultimate Behaviour of Prestressed Box Girder Cable Stayed Bridgesaper ." IOSR Journal of Mechanical and Civil Engineering (IOSR-JMCE) , vol. 16, no. 5, 2019, pp. 52-65